Erschienen in: European Journal of Inorganic Chemistry ; 2018 (2018), 6. - S. 713-721
https://dx.doi.org/10.1002/ejic.201701459

The $[Fe\{(SePPh_2)_2N\}_2]$ Complex Revisited: X-ray Crystallography, Magnetometry, High-Frequency EPR, and Mössbauer Studies Reveal Its Tetrahedral $Fe^{II}Se_4$ Coordination Sphere

Eleftherios Ferentinos,[a] Spyros Chatziefthimiou,[b][‡] Athanassios K. Boudalis,[b][‡‡] Michael Pissas,[b] Guinevere Mathies,[c][‡‡‡] Peter Gast,[c] Edgar J. J. Groenen,*[c] Yiannis Sanakis,*[b] and Panayotis Kyritsis*[a]

Abstract: The synthesis and characterization of complex $[Fe\{(SePPh_2)_2N\}_2]$ (**1**) is described. X-ray crystallography shows that this system contains a tetrahedral $FeSe_4$ coordination sphere. The structural features of **1** are compared with those of similar first row transition element complexes, including a recently reported preparation of $[Fe\{(SePPh_2)_2N\}_2]$ ($\mathbf{1_{SP}}$) exhibiting a highly unusual square planar $FeSe_4$ coordination sphere. The electronic structure of **1** was elucidated by magnetometry, high-frequency EPR, and Mössbauer spectroscopic studies, which reveal zero-field splitting (ZFS) parameters typical of high spin $S = 2$ tetrahedral Fe^{II} sites. Accurate ZFS parameters ($D = +8.22$ cm^{-1}, $E/D = 0.104$) were obtained by analysis of the EPR spectra and compared with those of the analogous $[Fe\{(SPPh_2)_2N\}_2]$ complex.

Introduction

Selenium exhibits a rich and intensively investigated biological chemistry.[1] In that respect, the bioinorganic chemistry of selenium, mainly expressed via coordination of either selenocystein (Se-Cys) or selenide (Se^{2-}) to transition metals in metalloproteins or synthetic analogues, has been extensively explored. More specifically, X-ray crystallography has revealed the coordination of Se-Cys to nickel in the Ni-Fe-Se hydrogenase,[2] as well as to molybdenum in the active site of formate dehydrogenase[3] and nicotinate dehydrogenase.[4] The Ni-Fe-Se hydrogenase has been employed for the photocatalytic production of H_2 under increased O_2 levels,[5] while chemical analogues of its active site have been investigated.[6] The effects of replacing Cys by Se-Cys have been investigated in various metalloproteins, such as metallothionein,[7] Cyt P_{450},[8] azurin,[9] and sulfite oxidase.[10] Moreover, sulfide S^{2-} has been replaced by selenide Se^{2-} in the iron-sulfur active site of numerous proteins,[11] like the [4Fe-4S] cluster of [FeFe]-hydrogenase[12a] (Se/S substitution has also been carried out in the [2Fe] cluster of the latter[12b]), the iron protein of nitrogenase,[13] the photosystem I polypeptide PsaC,[14] aconitase,[15] high potential iron-sulfur protein,[16] as well as [2Fe-2S][17] and 2[4Fe-4S] ferredoxins.[18]

As far as the synthetic bioinorganic chemistry of selenium is concerned, a range of multinuclear clusters containing iron coordinated to Se^{2-} and various thiols,[19] as well as tungsten-iron-sulfur/selenium clusters,[20] have been investigated by Holm and co-workers. The coordination of selenium to transition metals has also been explored by employing the so called dichalcogenidoimidodiphosphinato ligands, $R_2P(E)NHP(E')R'_2$ (E, E′ = O, S, Se, Te; R, R′ = alkyl or aryl groups).[21] Among this family of chelating ligands, $L = [Ph_2P(Se)NP(Se)Ph_2]^-$,[22] containing E = E′ = Se as donor atoms, and R = R′ = Ph as peripheral groups bonded to the P atoms of the P–N–P backbone, has afforded the following structurally characterized homoleptic complexes with first series transition metal ions (structures deposited in the Cambridge Structural Database, CSD[23]): octahedral $M^{III}L_3$, M = V,[24] Cr,[24] tetrahedral $M^{II}L_2$, M = Mn,[25] Co,[26] Zn,[27] square planar $Ni^{II}L_2$[28] and tetranuclear $[Cu^{I}_4L_3]BF_4$.[29]

With respect to the coordination of $[Ph_2P(Se)NP(Se)Ph_2]^-$ to Fe^{II}, it should first be noted that the following literature complexes have been shown, by X-ray crystallography, to unequivocally contain a tetrahedral $FeSe_4$ coordination sphere: $[N(CH_3CH_2)_4]_2[Fe(SePh)_4]$,[30] $[Fe(1,10\text{-phen})_3][Fe(SePh)_4]$,[31]

[a] *Inorganic Chemistry Laboratory, Department of Chemistry, National and Kapodistrian University of Athens, Panepistimiopolis 15771, Athens, Greece*
E-mail: kyritsis@chem.uoa.gr
http://users.uoa.gr/~kyritsis/home.html
[b] *Institute of Nanoscience and Nanotechnology, N.C.S.R. "Demokritos", Aghia Paraskevi 15310, Attiki, Greece*
E-mail: i.sanakis@inn.demokritos.gr
https://inn.demokritos.gr/en/prosopiko/i.sanakis
[c] *Huygens-Kamerlingh Onnes Laboratory, Department of Physics, Leiden University, Niels Bohrweg 2, 2333 CA Leiden, The Netherlands*
E-mail: groenen@physics.leidenuniv.nl
https://www.universiteitleiden.nl/en/staffmembers/edgar-groenen#tab-1
[‡] Present address: EMBL-Hamburg c/o Deutsches Elektronen-Synchrotron, Hamburg, Germany
[‡‡] Present address: Institut de Chimie de Strasbourg (UMR 7177, CNRS-Unistra), Université de Strasbourg, 4 rue Blaise Pascal, CS 90032, 67081 Strasbourg, France
[‡‡‡] Present address: Department of Chemistry, University of Konstanz, Universitätsstraße 10, 78464 Konstanz, Germany
Supporting information and ORCID(s) from the author(s) for this article are available on the WWW under https://doi.org/10.1002/ejic.201701459.

$[PPh_4]_2[Fe(Se_4)_2]$,[32] $[N(CH_3)_4]_2[Fe\{SeC(CH_3)_3\}_4]$,[33] [bis(1,3-di-*tert*-butyl-1*H*-imidazol-3-ium)]$_2[Fe(SePh)_4]$,[34] $[Fe\{(SeP\textit{i}Pr_2)_2N\}_2]$[35] and $[Fe(dmise)_4][BF_4]_2$, dmise = *N*,*N*′-dimethylimidazole-selone.[36] In addition, on the basis of spectroscopic and room temperature magnetometry studies, the $[Fe\{(SePPh_2)_2CH\}_2]$ complex, bearing a ligand which is similar to L, has been proposed to also contain a tetrahedral $FeSe_4$ core.[37] Based on the above, the recently reported crystal structure of a preparation of FeL_2 containing a square planar $FeSe_4$ coordination sphere (**1$_{SP}$**, CSD code FOMWIP)[38] was rather unexpected and prompted us to revisit the FeL_2 system.

X-ray crystallography revealed that our preparation of FeL_2 (**1**), presented herein, exhibits clearly a tetrahedral $FeSe_4$ coordination sphere. The magnetic and spectroscopic properties of **1** were investigated by magnetometry, as well as by IR, high-frequency EPR and Mössbauer spectroscopy. Comparisons are being made with the properties of **1$_{SP}$**[38] $[Fe\{(SeP\textit{i}Pr_2)_2N\}_2]$[35] and $[Fe\{(SPPh_2)_2N\}_2]$[39] complexes. Recent high-frequency EPR studies of the latter have revealed distinct $S = 2$ Fe^{II} sites, the spin-Hamiltonian parameters of which have been accurately determined.[39b] This complex is a synthetic analogue of the reduced form of the iron-sulfur protein rubredoxin, which contains a $[Fe(S\text{-}Cys)_4]$ active site.[40] To our best knowledge, replacement of the iron-coordinating Cys residues of rubredoxin by Se-Cys has not yet been reported.

In the following, the interplay between literature tetrahedral and square planar Fe^{II} complexes, including their spin states and Mössbauer spectroscopic signatures, is analyzed. Moreover, the effects on the *D* (axial) and *E* (rhombic) zero-field splitting (ZFS) components of Fe^{II} coordination to $[Ph_2P(Se)NP(Se)Ph_2]^-$, as opposed to $[Ph_2P(S)NP(S)Ph_2]^-$,[39b] in a similar tetrahedral $S = 2$ FeE_4 site, E = S, Se, are also discussed.

Results and Discussion

Chemical Synthesis

Complex **1** was synthesized by mixing $FeCl_2$ and the $[Ph_2P(Se)NP(Se)Ph_2]^-$ ligand, under anaerobic conditions, in order to minimize the formation of byproduct Fe^{III} species. A different preparation of the same complex (**1$_{SP}$**) has been recently reported.[38] The proposed crystal structure of **1$_{SP}$**, containing a square planar $FeSe_4$ coordination sphere, will be compared, in the following, with that of the present complex **1**.

X-ray Crystallography and IR Spectroscopy

The molecular structure of **1** is shown in Figure 1. The crystal data, as well as the refinement statistics, of the structure of **1** are listed in Table S1 (Supporting Information). Selected bond lengths and angles of **1**, are listed in Tables S2 and S3, respectively.

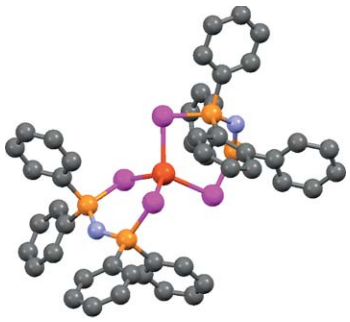

Figure 1. Molecular structure of complex **1**. The H atoms are omitted for clarity. Color coding: Iron (brown), selenium (magenta), phosphorus (light brown), nitrogen (blue), carbon (gray).

The $FeSe_4$ core of complex **1** exhibits a distorted tetrahedral geometry, as reflected by the magnitude of the Se–Fe–Se angles which lie between 101.7(1)° and 115.7(1)° (Table S2). The two endocyclic Se–Fe–Se bite angles amount to 115.7(1)° and are similar to those of the $[Fe\{(SeP\textit{i}Pr_2)_2N\}_2]$[35] and $[M\{(SePPh_2)_2N\}_2]$, M = Mn,[25] Co,[26] Zn,[27] complexes listed in Table 1. The dihedral angle between the planes defined by the endocyclic Se–Fe–Se angles of complex **1** is 86.8°, comparable to those of the $[M\{(SePPh_2)_2N\}_2]$, M = Mn, Co, Zn, complexes (Table 1). The significantly smaller values, 81.3° and 82.4°, respectively, for the sites 1 and 2 of the recently reported $[Fe\{(SeP\textit{i}Pr_2)_2N\}_2]$ complex reveal a more profound deviation from the value (90.0°) of the ideal tetrahedral structure, apparently imposed by the *i*Pr peripheral groups of the ligand. In addition, the latter structure exhibits a different space group compared with the rest of those listed in Table 1. The FeSePNPSe rings in the structure of **1** adopt a pseudo-boat conformation, with the P and Se atoms at the apices, in agreement with the structure of the analogous Mn, Co, Zn complexes (Table 1).

The averaged P–Se and P–N bond lengths of $Ph_2P(Se)NHP(Se)Ph_2$ and **1** are listed in Table 2. Close inspection reveals that the average P–Se bond length of **1** is increased compared with that of the ligand, whereas the opposite trend

Table 1. Selected structural parameters of $[M\{(SePPh_2)_2N\}_2]$, M = Mn, Fe, Co, Zn, and $[Fe\{(Se\textit{i}Pr_2)_2N\}_2]$ complexes.

ML_2	Av. M–Se [Å]	Endocyclic bite angle SeMSe [°]	Angle of endocyclic bite planes [°]	Space group	CSD code[23]
Fe (**1**)	2.48	115.7, 115.7	86.8	$P\bar{1}$	This work
$[Fe\{(Se\textit{i}Pr_2)_2N\}_2]$ site 1	2.47	112.4, 112.7	81.3	$P2_1$	CADQIK[35]
$[Fe\{(Se\textit{i}Pr_2)_2N\}_2]$ site 2	2.47	112.2, 112.7	82.4		
Mn	2.56	113.7, 112.8	87.4	$P\bar{1}$	DEJRUG[25]
Co	2.42	113.4, 114.1	89.2	$P\bar{1}$	LIXSIU[26b]
Co	2.43	114.3, 115.0	87.7	$P\bar{1}$	LIXSIU01[26a]
Zn	2.48	114.7, 115.9	88.0	$P\bar{1}$	ARIDEK[27]

Table 2. Average M–Se, P–Se, P–N bond lengths and P–N–P angles of the $Ph_2P(Se)NHP(Se)Ph_2$ ligand and complexes discussed in the text.

Ligand/Complex	Av. Fe–Se [Å]	Av. P–Se [Å]	Av. P–N [Å]	Endocyclic bite SeFeSe [°]	Av. PNP [°]	CSD code[23]
LH		2.05	1.69		132.0	YUSDUL[22]
1	2.48	2.16	1.59	115.7	133.9	This work
$[Fe\{(SeP^iPr_2)_2N\}_2]$						
Site 1	2.47	2.19	1.60	112.6	138.0	CADQIK[35]
Site 2	2.47	2.19	1.60	112.5	138.2	
$\mathbf{1_{SP}}$						
Site 1	2.66	2.17	1.58	88.4	138.8	FOMWIP[38]
Site 2	2.65	2.17	1.59	88.6	135.3	
S.P. $SnSe_4$						
Site 1	2.66	2.17	1.58	88.0	138.6	ZOPGEQ[41]
Site 2	2.65	2.18	1.58	88.4	136.2	
$[Se\{(SePPh_2)_2N\}_2]$						
Site 1	2.66	2.18	1.59	88.3	138.5	GEFHUK[42]
Site 2	2.65	2.18	1.59	88.7	136.3	

is observed for the average P–N bond length. These observations are in agreement with the findings based on the IR spectra of $Ph_2P(Se)NHP(Se)Ph_2$ and complex **1**. The IR spectrum of the former contains characteristic bands, which are attributed to the ν(PSe) (595, 546) and ν_{as}(PNP) (937, 926, 918) stretching vibrations, respectively.[22] On the other hand, in the IR spectrum of complex **1** the bands observed at 534 and 1203 cm^{-1} are assigned to the ν(PSe) and ν_{as}(PNP) stretching vibrations, respectively. The aforementioned IR data are compatible with an increase of the P–N bond order and a decrease of the P–Se bond order, upon coordination of the ligand to Fe^{II}. This trend has been observed before for similar metal complexes and is thought to be caused by the delocalization of π-electron density over the ligand framework upon its coordination to the metal center.[21c,25] The bond-order shifts suggested by the above IR data, confirm the structural differences between $Ph_2P(Se)NHP(Se)Ph_2$ and complex **1** observed by X-ray crystallography (vide supra). It should be noted that similar ν(PSe) and ν_{as}(PNP) stretching vibrations, respectively, have been reported for tetrahedral $[M\{(SePPh_2)_2N\}_2]$, M = Mn (536, 1205),[25] Co (545, 1199).[26b]

The average value of the four non-equivalent Fe–Se bond lengths of complex **1** is 2.48 Å (Table 2), which is within the corresponding values observed for tetrahedral $Fe^{II}Se_4$-containing complexes identified in the CSD:[23] $[N(CH_3CH_2)_4]_2[Fe(SePh)_4]$ (2.46 Å),[30] $[Fe(1,10\text{-phen})_3][Fe(SePh)_4]$ (2.46 Å),[31] $[PPh_4]_2[Fe(Se_4)_2]$ (2.45/2.43 Å),[32] $[N(CH_3)_4]_2[Fe\{SeC(CH_3)_3\}_4]$ (2.47 Å),[33] [bis(1,3-di-*tert*-butyl-1*H*-imidazol-3-ium)]$_2$[Fe(SePh)$_4$] (2.45 Å),[34] $[Fe\{(SeP^iPr_2)_2N\}_2]$ (2.47 Å)[35] and $[Fe(dmise)_4][BF_4]_2$, dmise = *N*,*N*′-dimethylimidazoleselone (2.46 Å).[36] The recently reported structure of $\mathbf{1_{SP}}$ surprisingly contains a square planar $FeSe_4$ coordination sphere.[38] This structure exhibits significantly larger average Fe–Se bond lengths (2.65 and 2.66 Å for its two sites, Table 2), compared with those of complex **1** and the above tetrahedral $FeSe_4$-containing complexes. These larger bond lengths are very similar to those of the initially suggested square planar $[Sn\{(SePPh_2)_2N\}_2]$ complex (S.P. $SnSe_4$, CSD code ZOPGEQ),[41] as well as that of structurally characterized $[Se\{(SePPh_2)_2N\}_2]$ (CSD GEFHUK)[42] (Table 2). In addition, the unit cell parameters of the FOMWIP, ZOPGEQ and GEFHUK structures, listed in Table S4, are rather similar. It should be stressed that an earlier report that the $[Sn\{(SePPh_2)_2N\}_2]$ complex contains a square planar $SnSe_4$ coordination sphere[41] has been extensively discussed, with suggestions that the reported crystal structure is due to crystals of $[Se\{(SePPh_2)_2N\}_2]$, presumably formed as a side-product during the synthesis of the Sn^{II} complex.[43] Attention should also be given to the fact that the cif file of the $\mathbf{1_{SP}}$ FOMWIP structure,[38] deposited in the CSD,[23] reports large calculated positive residual density on the Fe2 atom, which could be attributed to occupation of the metal site by the heavier Se atom.

It is of interest that square planar $Fe^{II}O_4$ sites have been found in solid-state structures,[44] including the rare mineral gillespite ($BaFe^{II}Si_4O_{10}$)[45] and a catalytically active Fe^{II} zeolite site converting methane to methanol.[46] On the other hand, only a handful of molecular Fe^{II} systems contain square planar FeO_4[44b,47] or FeO_2NCl[48] coordination spheres, and these are qualified as highly unusual.[47c] The above systems have been shown to contain high spin, $S = 2$, sites, exhibiting unique Mössbauer spectroscopic signatures (vide infra). Square planar complexes of Fe^{II} containing intermediate spin, $S = 1$, sites, have also been reported[49] (and references cited therein). In addition, Fe^{II}-porphyrins contain square-planar $Fe^{II}N_4$ coordination spheres exhibiting various spin states.[50] Complex $\mathbf{1_{SP}}$ has not been studied by either magnetometry or by any spectroscopic method.[38] On the other hand, the spin state ($S = 2$) and tetrahedral geometry of **1** reported herein is strongly supported by magnetometry and high-frequency EPR/Mössbauer spectroscopy (vide infra).

Based on the above observations, the FOMWIP square planar $Fe^{II}Se_4$ structure of $\mathbf{1_{SP}}$ needs to be re-examined, with respect to the possibility that it is due to crystals of $[Se\{(SePPh_2)_2N\}_2]$ formed as a by-product under the reaction conditions employed for its synthesis.[38] Although it is not possible to assess the validity of the deposited FOMWIP cif file, it is of interest that issues concerning the reliable validation of a CSD-deposited cif

file have been recently raised.[51] In addition, complex **1$_{SP}$** should also be investigated by magnetometry and spectroscopic methods, in order for its magnetic properties to be assessed in detail.

It is of interest that a case of stereoisomerism in a four-coordinate 3d metal complex has been observed for [Ni{(SeP*i*Pr$_2$)$_2$N}$_2$], which has been shown to afford discrete crystals containing tetrahedral and square planar NiSe$_4$ coordination spheres.[52] In this case, the square planar isomer exhibits shorter Ni–Se bond lengths, compared with those of the tetrahedral one, in agreement with expectations from ligand field theory for complexes containing a d^8 metal center like Ni^{II}.[53] Similar arguments have been put forward for tetrahedral and square planar organometallic complexes of Fe^{II}.[54] The fact that **1$_{SP}$** exhibits significantly larger Fe–Se bond lengths than **1** needs to be further discussed, once the spin state of **1$_{SP}$** has been unequivocally determined.

Magnetometry

The temperature dependence of the magnetic susceptibility χ_M of **1**, plotted as $\chi_M T$ vs. T recorded under a direct current (DC) field of 1 T, is shown in Figure 2. At high temperatures, the value of $\chi_M T$ is 3.59 cm^3 mol^{-1} K, which is consistent with an $S = 2$ species exhibiting $g > 2.0$. Upon cooling, the $\chi_M T$ product exhibits a very progressive and linear decrease down to 100 K. Upon further cooling, the decrease becomes more pronounced, reaching 1.19 cm^3 mol^{-1} K at 2 K. We attribute this behavior to the combined effects of magnetization saturation under the influence of the magnetic field due to Zeeman interactions and to ZFS effects. To better study the ZFS contributions, we carried out isothermal magnetization studies at 2, 3 and 5 K, which we plot as M vs. HT^{-1} in the inset of Figure 2.

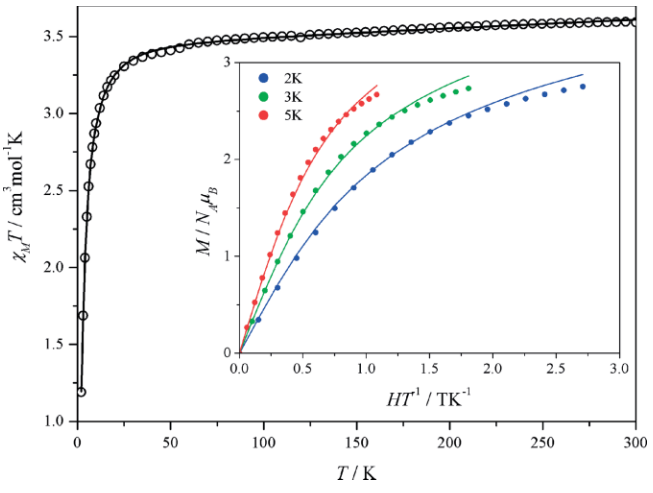

Figure 2. Temperature dependence of $\chi_M T$ of a powder sample of **1** under a magnetic field of 1 T. The inset shows isothermal magnetization data plotted as M vs. HT^{-1} at the indicated temperatures. Solid lines correspond to the best-fit solution described in the text.

Simultaneous fits were carried out on the $\chi_M T$ vs. T and the M vs. HT^{-1} data, using the spin Hamiltonian in Equation (1)

$$H = D[S_z^2 - S(S+1)/3] + E(S_x^2 - S_y^2) + \beta \mathbf{S}\mathbf{g}B \quad (1)$$

in which D and E are, respectively, the axial and rhombic components of ZFS, β is the Bohr magneton and B is the external magnetic field. For the analysis of the magnetic data, the g-tensor is assumed isotropic.

Models considering $D > 0$ and $D < 0$, as well as $E = 0$ and $E \neq 0$, were examined, corresponding to four different solutions. Best-fit parameters were $g_{iso} = 2.14$ (±0.02), $D = +7.9$ (±0.2) cm^{-1}, $E = +1.1$ (±0.5) cm^{-1}, *TIP* (*Temperature Independent Paramagnetism*) = 5.5 (±0.5) × 10^{-4} cm^3 mol^{-1} K. It is noteworthy that magnetic susceptibility, as well as isothermal magnetization data, was sensitive to the sign of D. As can be seen from the various solutions presented in Figures S1 and S2, it is clear that acceptable fits were only derived for $D > 0$. Moreover, liberating the E parameter in the case of $D > 0$, further improved these fits, yielding an E/D value of 0.14.

These results are in good agreement with high-frequency EPR measurements (vide infra). From the magnetometry data, it is already clear that complex **1** exhibits a rather large and positive D value. Therefore, as the $M_s = 0$ is the ground state of this $S = 2$ system, no significant slow relaxation of magnetization is expected. Indeed, Alternating Current (AC) magnetic susceptibility measurements (not shown), either in the absence or in the presence of a DC magnetic field, do not show a non-zero value of the imaginary part, χ'', of the magnetic susceptibility that would indicate slow relaxation of the magnetization.

High-Frequency EPR Spectroscopy

The cw EPR spectrum of a powder sample of **1** recorded at 275.7 GHz and 10 K is shown in Figure 3. The spectrum comprises several resonances, with the most relevant for the $S = 2$ Fe^{II} site of **1** being those at ca. 2.0, 4.7, 5.2 and 8.8 T. The signal around 9.8 T ($g = 2$) may arise from a high spin, $S = 5/2$, Fe^{III} species, whereas the signal at 9.6 T is due to an impurity in the cavity. Finally, a rather weak signal is observed at ca. 0.7 T, superimposed on a relatively broad background. The origin of the above features is discussed below.

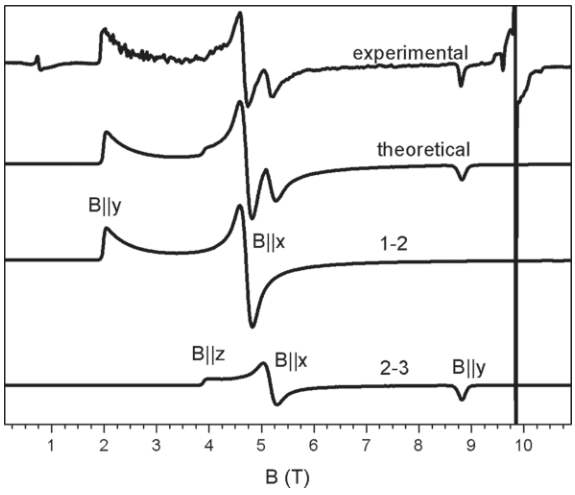

Figure 3. Experimental and theoretical 275.7 GHz cw-EPR spectra of a powder sample of **1** at 10 K. The theoretical spectra are obtained as described in the text. Experimental conditions: Modulation frequency: 1.8 kHz, modulation amplitude: 3 mT, microwave power: 5 μW.

The magnetic measurements presented above were satisfactorily analyzed within the spin Hamiltonian (1), yielding the spin Hamiltonian parameters presented above. A more reliable and accurate determination of these parameters is obtained by the analysis of the high-frequency EPR resonances. Figure S3 depicts the dependence of the energy levels on the external magnetic field, for three orientations with respect to the principal axes of the ZFS tensor, assuming the ZFS values that reproduce the spectra. On the basis of these plots, the resonance at about 2.0 T is attributed to the transition between the lowest lying levels 1 and 2 for an orientation of the magnetic field parallel to the *y*-axis, whereas the resonance at about 4.6 T is attributed to the transition between the lowest-lying levels for an orientation parallel to the *x*-axis. Similarly, the resonances at 5.0 T and 8.5 T arise from the next two levels, 2–3, with the orientation parallel to *x*- and *y*-axes, respectively. A weak shoulder at 4.0 T can be attributed to the 2–3 transition for an orientation parallel to the *z*-axis. A survey over the parameter space indicates that all transitions can be simultaneously reproduced with a unique set of parameters D, E/D, $g_\perp$, and $g_\parallel$ in a relatively narrow range (see Figure S4 and the corresponding analysis presented in the Supporting Information). In Figure 3 are included simulations of the spectra obtained with the following set of spin Hamiltonian parameters: D = +8.22 (±0.05) cm^{-1}, E/D = 0.104 (±0.010), $g_\perp$ = 2.12 (±0.01) and $g_\parallel$ = 2.10 (±0.01). The contribution from each transition between the levels 1–2 and 2–3 is shown separately. The fine structure between 2 and 4 T (Tesla) is not noise from the acquisition. This structure changes when the sample tube is rotated; this refers to the presence of microcrystals in the EPR sample that are remnants of the procedure of making a fine powder. These effects become visible due to the small volume of only 20 nL of the sample in the EPR cavity and the extreme width of the transition (>>2 T).

In Figure S5, a simulation of the EPR spectrum is shown, using the parameters determined by the analysis of the magnetometry data. Although the values derived by the two methods are close to each other, the higher sensitivity of EPR spectroscopy for systems like the one under study in this work, allows for a more accurate determination of the spin Hamiltonian parameters.

The spectra recorded at 10 and 25 K are compared in Figure S6. We observe that upon increasing the temperature, the relative intensity of the 2–3 signals increases with respect to the intensity of 1–2, in agreement with the above assignment, further confirming the positive sign of D. The signals at 9.6 T arise from an impurity species of the cavity, whereas the strong derivative feature at about 10 T can be attributed to half integer spin species, such as high spin, S = 5/2, Fe^{III} impurities. Less obvious is the origin of the signals in the low field (<1.0 T) part of the spectrum, which is enlarged in Figure S7. A closer examination indicates that the relatively sharp peak at 0.7 T is superimposed on a rather broad background. We tentatively assign these signals to the existence of two additional S = 2, high spin Fe^{II} minor species (see the caption of Figure S7). The origin of these minor species is at present unknown. In any case, quantification of these signals, with respect to the major S = 2 Fe^{II} signals, indicates that they represent a small fraction of total iron (ca. 3.0 %). These S = 2, Fe^{II} impurities with significant ZFS values do not affect critically the analysis of the magnetometry data, because the major species are also S = 2 species with large ZFS parameters. The magnetometry data, however, can be distorted by some high spin ferric impurities, as it is indicated by the sharp signal at about 10 T in the EPR spectrum. In Figure S8, we compare the $\chi_M T$ vs. T and M vs. HT^{-1} simulations, assuming the ZFS and ***g***-tensor parameters obtained by the analysis of the magnetometry data (vide supra) and those determined by EPR. The discrepancy can be adequately justified assuming a high spin, S = 5/2, Fe^{III} impurity of about 3 %. Both types of minor species could be hardly discernible in the Mössbauer spectra (vide infra).

The size of D for complex **1** is typical for high spin S = 2 Fe^{II} systems, including the, most relevant, analogous [Fe{(SPPh$_2$)$_2$N}$_2$] complex (ref.[39b] and references cited therein). This complex has been shown to adopt different structural conformations, the electronic structure of which exhibits subtle variations. More specifically, the corresponding ZFS parameters of two distinct conformations are D_1 = +9.17 cm^{-1}, E_1/D_1 = 0.021 and D_2 = +8.87 cm^{-1}, E_2/D_2 = 0.052. The D component of the ZFS of **1** is comparable to those of each distinct site of [Fe{(SPPh$_2$)$_2$N}$_2$], while the value of E/D is slightly bigger, suggesting that the nature of the ligand's donor atom (S vs. Se) has a small effect on the ZFS for the corresponding S = 2 Fe^{II}E$_4$, E = S, Se, tetrahedral sites. It should be stressed that recent magnetometry studies have provided evidence that the high spin S = 3/2 tetrahedral [Co{(EP*i*Pr$_2$)$_2$N}$_2$], E = S, Se, complexes also exhibit rather similar (ca. –30 cm^{-1}) D values, i.e. the magnitude of D does not depend on the identity of the E donor atoms (S or Se) in these systems as well.[55]

Mössbauer Spectroscopy

Zero-field Mössbauer spectra of powder samples of **1** were recorded in the 4.2–200 K temperature range. The spectra at 4.2 and 80 K are shown in Figure 4. The spectra comprise one quadrupole doublet and the corresponding Mössbauer parameters are listed in Table S5. Spectra recorded at various other temperatures are shown in Figure S9.

The spectrum at 4.2 K comprises one symmetric doublet, exhibiting the following parameters: δ = 0.79(1) mm s^{-1} and $|\Delta E_Q|$ = 3.23(1) mm s^{-1}. These parameters are fully consistent with a high spin S = 2 Fe^{II} site.[56] In particular, the magnitude of the quadrupole splitting provides conclusive evidence that **1** contains a tetrahedral coordination sphere. High spin, S = 2, square-planar Fe^{II} sites are rather rare (vide supra). Among this family of Fe^{II} systems, those that have been studied by Mössbauer spectroscopy[44b,48,50a,57] exhibit quadrupole doublets with remarkably low $|\Delta E_Q|$ values (<< 1.0 mm s^{-1}). This trend, which has also been observed for S = 2, trigonal planar Fe^{II} sites with thiolate ligands,[58] may be qualitatively understood on the basis of the symmetry of the square planar ligand environment. Under these conditions, the contribution of the ligand environment to the electric field gradient (EFG) tensor cancels out the contribution of the valence, thus leading to unusually small, for S = 2 Fe^{II} sites, $|\Delta E_Q|$ values.[59] On the other hand, in tetrahedral

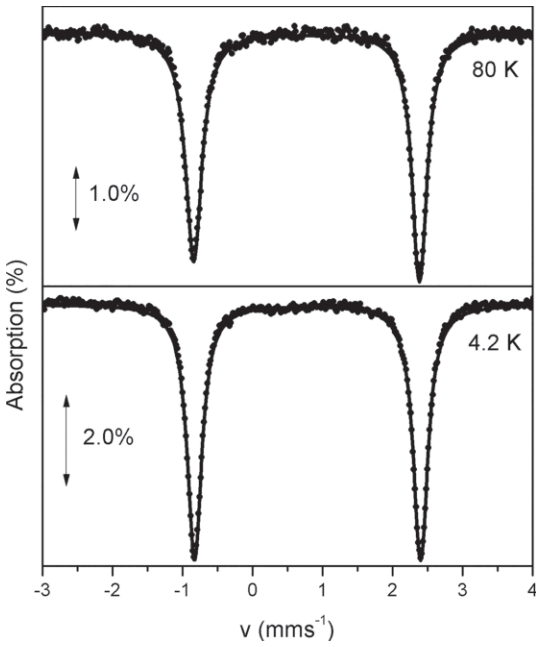

Figure 4. Zero-field Mössbauer spectra of a powder sample of **1** at 4.2 and 80 K. Solid lines are theoretical simulations, as described in the text.

ligand environments, the ligand asymmetry contribution to the EFG tensor is much smaller and, therefore, the valence contribution prevails, leading to the usual large $|\Delta E_Q|$ values for such $S = 2$ Fe^{II} sites. Most relevant to the case of complex **1** are the recently studied tetrahedral $[Fe\{(SeP{i}Pr_2)_2N\}_2]$, E = S, Se, complexes.[35] These complexes exhibit, within experimental error, δ and $|\Delta E_Q|$ values of the same order of magnitude with those of complex **1**. The $|\Delta E_Q|$ parameter of complex **1** exhibits a non-profound temperature dependence (Figure S9), implying a well isolated orbital ground state.

At 4.2 K, the observed doublet of **1** is symmetric with Lorentzian lines. The linewidth (FWHM, $\Gamma = 0.25$ mm s^{-1}) is close to the lowest limit of our experimental setup. This indicates a well-defined and fairly homogeneous ligand environment of the Fe^{II} center in complex **1**. The minor $S = 2$, Fe^{II} species, suggested by EPR, could not induce recognizable distortion of this doublet. Within the available signal to noise ratio, some anomalies in the background in the 0–1 mm s^{-1} region can be attributed to $S = 5/2$, Fe^{III} impurities. The inherent narrowness of the lines makes it possible to detect small, albeit reliable, changes as a function of temperature. As the temperature increases, the quadrupole doublet is getting asymmetric, with the lowest energy line becoming broader than the highest energy line. The largest asymmetry is observed at 80 K (Figure 4). A similar behavior has been observed in other $S = 2$ Fe^{II} systems[60] and it may be understood on the basis of relaxation effects.[61] High-frequency EPR and magnetometry studies show that the D value of complex **1** is rather large and positive, of the order of +8.0 cm^{-1} (vide supra). This corresponds to an $M_s = 0$ ground state, designated as |0>, which is separated by $D \approx 8$ cm^{-1} from the first excited |±1> and $4D \approx 32$ cm^{-1} from the second excited |±2> non-Kramers doublet, respectively. At 4.2 K, the thermal population of the ground |0> state is about 88.5 %. Therefore, no magnetic field is induced on the ^{57}Fe nucleus and the spectrum gives rise to a doublet. The non-zero rhombic E component of the ZFS revealed by the high-frequency EPR studies splits further the |±1> first excited doublet (about 11.5 % population at 4.2 K) into two singlets, which do not induce effective magnetic fields at the nucleus either. The splitting of the |±2> excited non-Kramers doublet is much smaller and, under favorable spin relaxation conditions, this state can give rise to magnetically split spectra. However, its thermal occupation at 4.2 K is negligible and does not affect the spectra. As the temperature increases, the occupation of the |±2> doublet increases. If the spin-lattice-relaxation time is appropriate (of the order of 10^{-7} s), this doublet will affect the spectra, resulting in asymmetric broadening. At 80 K, the occupation of the |±2> doublet is sufficiently large (ca. 29 %) and the relaxation effects are observable through the asymmetric broadening of the doublet. At higher temperatures, the occupation of the |±2> doublet reaches a saturation value and then the spin-relaxation time decreases. Under these conditions, the quadrupole doublet is becoming more symmetric again.

The zero-field Mössbauer spectra of complex **1** recorded at various temperatures (Table S5, Figure S9) are consistent with the findings of the magnetometry and high-frequency EPR studies, which indicate a large and positive ZFS axial component, D (vide supra).

Conclusions

In this work, the synthesis and characterization of a preparation of $[Fe\{(SePPh_2)_2N\}_2]$ (**1**) is described. X-ray crystallography shows that this system contains a tetrahedral $FeSe_4$ coordination sphere. The electronic structure of **1** is elucidated by magnetometry, high-frequency EPR and Mössbauer spectroscopy studies, which provide spin Hamiltonian parameters typical of high spin, $S = 2$, tetrahedral Fe^{II} sites. The magnitude of the D parameter is similar to that of the corresponding $[Fe\{(SPPh_2)_2N\}_2]$ complex. The recently reported preparation of $[Fe\{(SePPh_2)_2N\}_2]$ ($\mathbf{1_{SP}}$) exhibiting a square-planar coordination sphere should be investigated in a similar manner, in order to establish magnetostructural correlations for this system.

Experimental Section

Reagents and Synthetic Procedures: All manipulations were carried out under a pure Ar atmosphere, by employing Schlenk techniques. The $Ph_2P(Se)NHP(Se)Ph_2$ ligand was prepared according to published procedures.[22]

Complex 1: In a Schlenk-type flask, 0.032 g (0.25 mmol) $FeCl_2$ were added to a solution of 0.29 g (0.50 mmol) $K[(SePPh_2)_2N]$ in dry CH_3OH (30 mL) affording a pale yellow solid. The mixture was stirred for 2 h at room temperature and after that the solvent was removed to dryness under vacuum. CH_2Cl_2 (10 mL) was then added, followed by filtration through Celite pad in order to remove KCl that is formed. Suitable dark yellow crystals for X-ray crystallography were obtained by slow mixing of *n*-hexane layer to the above CH_2Cl_2 filtrate. Elemental analysis: calcd. C 50.55, H 3.54, N 2.46;

found C 50.25, H 3.50, N 2.46. Selected IR bands: ν(PSe) 534, ν_{as}(PNP) 1203 cm^{-1}.

X-ray Crystallography

Diffraction data were collected at room temperature, by the θ-2θ scanning method on a Syntex diffractometer equipped with Rigaku rotating anode and graphite monochromator [Cu-K_α radiation (λ= 1.5418 Å)]. The cell dimensions were obtained by least-squares analysis of reflections in the range 20° < 2θ < 40°. Three standard reflections were monitored every 97 reflections, showing no decay in intensity during data collection. The data were corrected for Lorentz and polarization effects and a semiempirical absorption correction, based on the psi scans, was applied.[62] The structure was solved by direct methods and refined by full-matrix least-squares based on F^2, using the program SHELXL97.[63] Anisotropic refinement was applied to all non-hydrogen atoms. Hydrogen atoms have been placed in idealized positions and refined by the riding model (UH = 1.20 UC).

CCDC 1574747 (for **1**) contains the supplementary crystallographic data for this paper. These data can be obtained free of charge from The Cambridge Crystallographic Data Centre.

The structure of **1** shown in Figure 1 was visualized by employing the CSD Mercury software (https://www.ccdc.cam.ac.uk/solutions/csd-system/components/mercury/).

IR Spectroscopy: IR spectra were run in the range 4000–200 cm^{-1} on a PERKIN-ELMER 883 IR spectrophotometer, as KBR discs.

Magnetometry: Magnetic susceptibility measurements were performed using an MPMS-5500 Quantum Design (for dc measurements) or a Quantum Design PPMS (for ac or dc measurements) magnetometers. Experimental data were corrected for the sample holder and for the diamagnetic contribution of the sample using Pascal's constants. The PHI program (v 3.1) was used for fitting the magnetic data.[64]

High-Frequency EPR Spectroscopy

Continuous-wave (cw) EPR spectra were recorded at 275.7 GHz using a home-built spectrometer at Leiden University,[65] using a probe specially developed to record the extremely broad spectra of high spin Fe-systems in cw mode.[66] A TE_{011} resonator was used for detection of the EPR signal allowing a sample volume of 20 nL. Spectra of **1** were recorded with a field-modulation amplitude of 3 mT, a modulation frequency of 1.8 kHz, and a microwave power of 5 μW.

Simulations of the EPR powder spectra were performed by numerical diagonalization of the spin Hamiltonian with the help of the EasySpin toolbox for Matlab,[67] or with the program SpinCount, kindly provided to us by Prof. M. P. Hendrich, Carnegie Mellon University, Pittsburgh, PA, U.S.A.

Mössbauer Spectroscopy: Mössbauer spectra were recorded by a constant-acceleration conventional spectrometer with a source of ^{57}Co (Rh matrix). Spectra were obtained using a Janis or an Oxford cryostat. The spectra were analyzed by using home written routines. Isomer shift values (δ) are reported relative to iron foil at 293 K.

Supporting Information (see footnote on the first page of this article): Crystal data and crystallographic information files, selected bond lengths and angles, structural comparisons, magnetometry/EPR/Mössbauer data for complex **1**.

Acknowledgments

E. F. has been awarded a State Scholarship Foundation (IKY) fellowship, by the act "Support for Postdoctoral Researchers", from the operational program "Human Power Development, Education and Lifelong Learning" (6, 8, 9 priority axes), co-funded by the European Social Fund and the Greek State. M. P. and Y. S. acknowledge support by the "Action for the Strategic Development on the Research and Technological Sector", funded by the Operational Programme "Competitiveness, Entrepreneurship and Innovation" and co-financed by the Greek State and the European Union (European Regional Development Fund; project MIS 5002567; NSRF 2014-2020). Dr. I. M. Mavridis is thanked for use of X-ray diffraction facilities at the Institute of Nanoscience and Nanotechnology, N.C.S.R. "Demokritos". Y. S. and P. K. participate in the activities of the Cost Action CM1305 (ECOSTBio), and they thank the rest of the ECOSTBio members for helpful discussions. We thank the reviewers of the manuscript for their constructive comments.

Keywords: Iron · Selenium · Imidodiphosphinato ligands · Structure elucidation · Magnetic properties

[1] a) R. Mousa, R. N. Dardashti, N. Metanis, *Angew. Chem. Int. Ed.* **2017**, *56*, 15818–15827; *Angew. Chem.* **2017**, *129*, 16027; b) N. Metanis, D. Hilvert, *Curr. Opin. Chem. Biol.* **2014**, *22*, 27–34; c) Y. Zhang, V. N. Gladyshev, *Chem. Rev.* **2009**, *109*, 4828–4861; d) D. L. Hatfield, P. A. Tsuji, B. A. Carlson, V. N. Gladyshev, *Trends Biochem. Sci.* **2014**, *39*, 112–120; e) L. A. Wessjohann, A. Schneider, M. Abbas, W. Brandt, *Biol. Chem.* **2007**, *388*, 997–1006.

[2] a) E. Garcin, X. Vernede, E. C. Hatchikian, A. Volbeda, M. Frey, J. C. Fontecilla-Camps, *Struct. Fold. Des.* **1999**, *7*, 557–566; b) C. S. A. Baltazar, M. C. Marques, C. M. Soares, A. M. DeLacey, I. A. C. Pereira, P. M. Matias, *Eur. J. Inorg. Chem.* **2011**, 948–962.

[3] J. C. Boyington, V. N. Gladyshev, S. V. Khangulov, T. C. Stadtman, P. D. Sun, *Science* **1997**, *275*, 1305–1308.

[4] N. Wagener, A. J. Pierik, A. Ibdah, R. Hille, H. Dobbek, *Proc. Natl. Acad. Sci. USA* **2009**, *106*, 11055–11060.

[5] a) T. Sakai, D. Mersch, E. Reisner, *Angew. Chem. Int. Ed.* **2013**, *52*, 12313–12316; *Angew. Chem.* **2013**, *125*, 12539; b) D. W. Wakerley, E. Reisner, *Energy Environ. Sci.* **2015**, *8*, 2283–2295.

[6] a) C. Wombwell, E. Reisner, *Chem. Eur. J.* **2015**, *21*, 8096–8104; b) C. Wombwell, E. Reisner, *Dalton Trans.* **2014**, *43*, 4483–4493; c) C. Wombwell, C. A. Caputo, E. Reisner, *Acc. Chem. Res.* **2015**, *48*, 2858–2865.

[7] T. Oikawa, N. Esaki, H. Tanaka, K. Soda, *Proc. Natl. Acad. Sci. USA* **1991**, *88*, 3057–3059.

[8] a) S. Cohen, D. Kumar, S. Shaik, *J. Am. Chem. Soc.* **2006**, *128*, 2649–2653; b) C. Aldag, I. A. Gromov, I. Garcia-Rubio, K. von Koenig, I. Schlichting, B. Jaun, D. Hilvert, *Proc. Natl. Acad. Sci. USA* **2009**, *106*, 5481–5486; c) Y. Y. Jiang, S. Sivaramakrishnan, T. Hayashi, S. Cohen, P. Moenne-Loccoz, S. Shaik, P. R. O. de Montellano, *Angew. Chem. Int. Ed.* **2009**, *48*, 7193–7195; *Angew. Chem.* **2009**, *121*, 7329; d) S. Sivaramakrishnan, H. Ouellet, J. Du, K. J. McLean, K. F. Medzihradszky, J. H. Dawson, A. W. Munro, P. R. O. de Montellano, *Biochemistry* **2011**, *50*, 3014–3024.

[9] a) S. M. Berry, M. D. Gieselman, M. J. Nilges, W. A. van der Donk, Y. Lu, *J. Am. Chem. Soc.* **2002**, *124*, 2084–2085; b) M. Ralle, S. M. Berry, M. J. Nilges, M. D. Gieselman, W. A. van der Donk, Y. Lu, N. J. Blackburn, *J. Am. Chem. Soc.* **2004**, *126*, 7244–7256; c) R. Sarangi, S. I. Gorelsky, L. Basumallick, H. J. Hwang, R. C. Pratt, T. D. P. Stack, Y. Lu, K. O. Hodgson, B. Hedman, E. I. Solomon, *J. Am. Chem. Soc.* **2008**, *130*, 3866–3877.

[10] S. Reschke, D. Niks, H. Wilson, K. G. V. Sigfridsson, M. Haumann, K. V. Rajagopalan, R. Hine, S. Leimkuehler, *Biochemistry* **2013**, *52*, 8295–8303.

[11] J. Meyer, J.-M. Moulis, J. Gaillard, M. Lutz, *Adv. Inorg. Chem.* **1992**, *38*, 73–115.

[12] a) J. Noth, J. Esselborn, J. Güldenhaupt, A. Brünje, A. Sawyer, U.-P. Apfel, K. Gerwert, E. Hofmann, M. Winkler, T. Happe, *Angew. Chem. Int. Ed.* **2016**, *55*, 8396–8400; *Angew. Chem.* **2016**, *128*, 8536; b) L. Kertessa, F. Wittkampb, C. Sommerc, J. Esselborna, O. Rudigerc, E. J. Reijersec, E. Hofmannd, W. Lubitzc, M. Winklera, T. Happea, U.-P. Apfelb, *Dalton Trans.* **2017**, *46*, 16947–16958.

[13] P. C. Hallenbeck, G. N. George, R. C. Prince, R. N. F. Thorneley, *J. Biol. Inorg. Chem.* **2009**, *14*, 673–682.

[14] Y. S. Jung, I. R. Vassiliev, J. H. Golbeck, *J. Biol. Inorg. Chem.* **1997**, *2*, 209–217.

[15] J. L. Breton, J. A. Farrar, M. C. Kennedy, H. Beinert, A. J. Thomson, *Biochem. J.* **1995**, *311*, 197–202.

[16] K. Govindaraju, J.-M. Moulis, G. A. Salmon, A. G. Sykes, *J. Chem. Soc., Dalton Trans.* **1993**, 643–647.

[17] a) M. W. W. Adams, K. K. Rao, D. O. Hall, G. Christou, C. D. Garner, *Biochim. Biophys. Acta* **1980**, *589*, 1–9; b) J. A. Fee, S. G. Mayhew, G. Palmer, *Biochim. Biophys. Acta* **1971**, *245*, 196–200; c) S. P. W. Tang, T. G. Spiro, K. Mukai, T. Kimura, *Biochem. Biophys. Res. Commun.* **1973**, *53*, 869–874; d) G. S. Wilson, J. C. M. Tsibris, I. C. Gunsalus, *J. Biol. Chem.* **1973**, *248*, 6059–6061; e) S. Benini, S. Ciurli, C. Luchinat, *Inorg. Chem.* **1995**, *34*, 417–420; f) J. Meyer, J.-M. Moulis, M. Lutz, *Biochim. Biophys. Acta* **1986**, *871*, 243–249.

[18] a) S. J. George, A. J. Thomson, D. E. Crabtree, J. Meyer, J.-M. Moulis, *New J. Chem.* **1991**, *15*, 455–465; b) J.-M. Moulis, J. Meyer, M. Lutz, *Biochemistry* **1984**, *23*, 6605–6613; c) J.-M. Moulis, J. Meyer, *Biochemistry* **1982**, *21*, 4762–4771.

[19] a) S. B. Yu, G. C. Papaefthymiou, R. H. Holm, *Inorg. Chem.* **1991**, *30*, 3476–3485; b) C. Y. Zhou, R. H. Holm, *Inorg. Chem.* **1997**, *36*, 4066–4077.

[20] B. Zheng, X. D. Chen, S. L. Zheng, R. H. Holm, *J. Am. Chem. Soc.* **2012**, *134*, 6479–6490.

[21] a) J. D. Woollins, *J. Chem. Soc., Dalton Trans.* **1996**, 2893–2901; b) T. Q. Ly, J. D. Woollins, *Coord. Chem. Rev.* **1998**, *176*, 451–481; c) C. Silvestru, J. E. Drake, *Coord. Chem. Rev.* **2001**, *223*, 117–216; d) I. Haiduc, "Dichalcogenoimidodiphosphinato Ligands" in *ComprehensiveCoordination Chemistry II: From Biology to Nanotechnology* (Eds.: J. A. McCleverty, T. J. Meyer), **2004**, Elsevier, Amsterdam, vol. 1, pp. 323–347; e) T. Chivers, J. S. Ritch, S. D. Robertson, J. Konu, H. M. Tuononen, *Acc. Chem. Res.* **2010**, *43*, 1053–1062; f) A. Grigoropoulos, D. Maganas, D. Symeonidis, P. Giastas, A. R. Cowley, P. Kyritsis, G. Pneumatikakis, *Eur. J. Inorg. Chem.* **2013**, 1170–1183.

[22] P. Bhattacharyya, J. Novosad, J. Phillips, A. M. Z. Slawin, D. J. Williams, J. D. Woollins, *J. Chem. Soc., Dalton Trans.* **1995**, 1607–1613.

[23] a) C. R. Groom, F. H. Allen, *Angew. Chem. Int. Ed.* **2014**, *53*, 662–671; *Angew. Chem.* **2014**, *126*, 675–684; b) F. H. Allen, *Acta Crystallogr., Sect. B* **2002**, *58*, 380–388.

[24] V. Bereau, P. Sekar, C. C. McLauchlan, J. A. Ibers, *Inorg. Chim. Acta* **2000**, *308*, 91–96.

[25] D. Maganas, S. S. Staniland, A. Grigoropoulos, F. White, S. Parsons, N. Robertson, P. Kyritsis, G. Pneumatikakis, *Dalton Trans.* **2006**, 2301–2315.

[26] a) L. M. Gilby, B. Piggott, *Polyhedron* **1999**, *18*, 1077–1082; b) J. Novosad, M. Necas, J. Marek, P. Veltsistas, C. Papadimitriou, I. Haiduc, M. Watanabe, J. D. Woollins, *Inorg. Chim. Acta* **1999**, *290*, 256–260.

[27] M. Afzaal, D. Crouch, M. A. Malik, M. Motevalli, P. O'Brien, J. H. Park, J. D. Woollins, *Eur. J. Inorg. Chem.* **2004**, 171–177.

[28] C. Papadimitriou, P. Veltsistas, J. Novosad, R. Cea-Olivares, A. Toscano, P. G. Y. Garcia, M. Lopez-Cardosa, A. M. Z. Slawin, J. D. Woollins, *Polyhedron* **1997**, *16*, 2727–2729.

[29] H. Z. Liu, N. A. G. Bandeira, M. J. Calhorda, M. G. B. Drew, V. Felix, J. Novosad, F. F. de Biani, P. Zanello, *J. Organomet. Chem.* **2004**, *689*, 2808–2819.

[30] J. M. McConnachie, J. A. Ibers, *Inorg. Chem.* **1991**, *30*, 1770–1773.

[31] A. Eichhoefer, G. Buth, F. Dolci, K. Fink, R. A. Mole, P. T. Wood, *Dalton Trans.* **2011**, *40*, 7022–7032.

[32] K. W. Kim, J. Kim, *Z. Kristallogr. New Cryst. Struct.* **2014**, *229*, 31–34.

[33] U. Florke, B. Hammann, G. Henkel, Cambridge Structural Database Communication, **2016**.

[34] T. Pugh, R. A. Layfield, *Dalton Trans.* **2014**, *43*, 4251–4254.

[35] N. Levesanos, W. P. R. Liyanage, E. Ferentinos, G. Raptopoulos, P. Paraskevopoulou, Y. Sanakis, A. Choudhury, P. Stavropoulos, M. Nath, P. Kyritsis, *Eur. J. Inorg. Chem.* **2016**, 5332–5339.

[36] B. S. Stadelman, M. M. Kimani, C. A. Bayse, C. D. McMillena, J. L. Brumaghim, *Dalton Trans.* **2016**, *45*, 4697–4711.

[37] A. Davison, D. L. Reger, *Inorg. Chem.* **1971**, *10*, 1967–1970.

[38] M. Akhtar, M. A. Malik, J. Raftery, P. O'Brien, *J. Mater. Chem. A* **2014**, *2*, 20612–20620.

[39] a) A. Davison, E. S. Switkes, *Inorg. Chem.* **1971**, *10*, 837–842; b) G. Mathies, S. D. Chatziefthimiou, D. Maganas, Y. Sanakis, S. Sottini, P. Kyritsis, E. J. J. Groenen, *J. Magn. Reson.* **2012**, *224*, 94–100.

[40] J. Meyer, J.-M Moulis in *Handbook of Metalloproteins*, John Wiley & Sons, **2006**.

[41] R. Cea-Olivares, J. Novosad, J. D. Woollins, A. M. Z. Slawin, V. Garcia-Montalvo, G. Espinosa-Perez, P. G. Y. Garcia, *Chem. Commun.* **1996**, 519–520.

[42] R. Cea-Olivares, G. Canseco-Melchor, V. García-Montalvo, S. Hernández-Ortega, J. Novosad, *Eur. J. Inorg. Chem.* **1998**, 1573–1576.

[43] E. Rufino-Felipe, E. Osorio, G. Merino, M. A. Munoz-Hernandez, *Dalton Trans.* **2013**, *42*, 11180–11185.

[44] a) Y. Tsujimoto, C. Tassel, N. Hayashi, T. Watanabe, H. Kageyama, K. Yoshimura, M. Takano, M. Ceretti, C. Ritter, W. Paulus, *Nature* **2007**, *450*, 1062–1065; b) D. Pinkert, S. Demeshko, F. Schax, B. Braun, F. Meyer, C. Limberg, *Angew. Chem. Int. Ed.* **2013**, *52*, 5155–5158; *Angew. Chem.* **2013**, *125*, 5260.

[45] A. Pabst, *Amer. Mineral.* **1943**, *28*, 372–390.

[46] B. E. R. Snyder, P. Vanelderen, M. L. Bols, S. D. Hallaert, L. H. Bottger, L. Ungur, K. Pierloot, R. A. Schoonheydt, B. F. Sels, E. I. Solomon, *Nature* **2016**, *536*, 317–321.

[47] a) X. Wurzenberger, H. Piotrowski, P. Klufers, *Angew. Chem. Int. Ed.* **2011**, *50*, 4974–4978; *Angew. Chem.* **2011**, *123*, 5078; b) S. A. Cantalupo, S. R. Fiedler, M. P. Shores, A. L. Rheingold, L. H. Doerrer, *Angew. Chem. Int. Ed.* **2012**, *51*, 1000–1005; *Angew. Chem.* **2012**, *124*, 1024; c) P. L. Holland, *Nat. Chem.* **2011**, *3*, 507–508.

[48] a) M. E. Pascualini, N. V. Di Russo, A. E. Thuijs, A. Ozarowski, S. A. Stoian, K. A. Abboud, G. Christou, A. S. Veige, *Chem. Sci.* **2015**, *6*, 608–612; b) M. E. Pascualini, S. A. Stoian, A. Ozarowski, K. A. Abboud, A. S. Veige, *Inorg. Chem.* **2016**, *55*, 5191–5200.

[49] Y. S. Liu, L. Luo, J. Xiao, L. Wang, Y. Song, J. P. Qu, Y. Luo, L. Deng, *Inorg. Chem.* **2015**, *54*, 4752–4760.

[50] a) J. R. Sams, T. B. Tsin, *Chem. Phys. Lett.* **1974**, *25*, 599–601; b) M. S. Liao, J. D. Watts, M. J. Huang, *J. Phys. Chem. A* **2007**, *111*, 5927–5935; c) O. K. Medhi, J. Silver, *Inorg. Chim. Acta* **1989**, *166*, 129–133.

[51] A. L. Spek, *Inorg. Chim. Acta* **2018**, *470*, 232–237.

[52] a) N. Levesanos, S. D. Robertson, D. Maganas, C. P. Raptopoulou, A. Terzis, P. Kyritsis, T. Chivers, *Inorg. Chem.* **2008**, *47*, 2949–2951; b) A. Panneerselvam, C. Q. Nguyen, J. Waters, M. A. Malik, P. O'Brien, J. Raftery, M. Helliwell, *Dalton Trans.* **2008**, 4499–4506.

[53] a) D. M. P. Mingos, *Essentials of Inorganic Chemistry 2*, Oxford University Press, New York, **1998**, p. 15; b) K. F. Purcell, J. C Kotz, *Inorganic Chemistry*, Saunders, London, **1977**, pp. 543–551; c) B. N. Figgis, M. A. Hitchman, *Ligand Field Theory and Its Applications*, Wiley-VCH, New York, **2000**, pp. 53–82.

[54] E. J. Hawrelak, W. H. Bernskoetter, E. Lobkovsky, G. T. Yee, E. Bill, P. J. Chirik, *Inorg. Chem.* **2005**, *44*, 3103–3111.

[55] S. Sottini, G. Poneti, S. Ciattini, N. Levesanos, E. Ferentinos, J. Krzystek, L. Sorace, P. Kyritsis, *Inorg. Chem.* **2016**, *55*, 9537–9548.

[56] N. N. Greenwood, T. C. Gibb, *Mössbauer Spectroscopy*, Chapman and Hall Ltd., London, UK, **1971**.

[57] a) N. Manicke, S. Hoof, M. Keck, B. Braun-Cula, M. Feist, C. Limberg, *Inorg. Chem.* **2017**, *56*, 8554–8561; b) M. G. Clark, G. M. Bancroft, A. J. Stone, *J. Chem. Phys.* **1967**, *47*, 4250–4261; c) D. Pinkert, M. Keck, S. G. Tabrizi, C. Herwig, F. Beckmann, B. Braun-Cula, M. Kaupp, C. Limberg, *Chem. Commun.* **2017**, *53*, 8081–8084.

[58] F. M. Macdonnell, K. Ruhlandtsenge, J. J. Ellison, R. H. Holm, P. P. Power, *Inorg. Chem.* **1995**, *34*, 1815–1822.

[59] Y. Sanakis, P. P. Power, A. Stubna, E. Munck, *Inorg. Chem.* **2002**, *41*, 2690–2696.

[60] Y. Calage, R. Tortevois, F. Varret, *J. Phys. Chem. Solids* **1990**, *51*, 911–913.

[61] D. C. Price, *Hyperfine Interact.* **1988**, *39*, 93–105.

[62] A. C. T. North, D. C. Phillips, F. S. Mathews, *Acta Crystallogr., Sect. A* **1968**, *24*, 351–359.
[63] G. M. Sheldrick, *SHELXL97*; University of Goettingen, Goettingen, Germany, **1997**.
[64] N. F. Chilton, R. P. Anderson, L. D. Turner, A. Soncini, K. S. Murray, *J. Comput. Chem.* **2013**, *34*, 1164–1175.
[65] H. Blok, J. Disselhorst, S. B. Orlinskii, J. Schmidt, *J. Magn. Reson.* **2004**, *166*, 92–99.
[66] G. Mathies, H. Blok, J. Disselhorst, P. Gast, H. van der Meer, D. M. Miedema, R. M. Almeida, J. J. G. Moura, W. R. Hagen, E. J. J. Groenen, *J. Magn. Reson.* **2011**, *210*, 126–132.
[67] S. Stoll, A. Schweiger, *J. Magn. Reson.* **2006**, *178*, 42–55.